A Geometry-based 3D Non-stationary UAV-MIMO Channel Model Allowing 3D Arbitrary Trajectories

Kaili Jiang*, Xiaomin Chen*, Qiuming Zhu*†, Weizhi Zhong‡, Yawen Wang*, Xiangbin Yu*, Bing Chen§
*College of Electronic and Information Engineering, Nanjing University of Aeronautics and Astronautics, Nanjing,211106, China
†Institute of Sensors, Signals and Systems, School of Engineering & Physical Sciences, Heriot-Watt University, Edinburgh, EH14 4AS, U.K.
‡College of Astronautics, Nanjing University of Aeronautics and Astronautics, Nanjing,211106, China
§College of Computer Science and Technology, Nanjing University of Aeronautics and Astronautics, Nanjing,211106, China
Email: {jiangkaili, chenxm402, zhuqiuming, zhongwz, wangyawen366, cb_china}@nuaa.edu.cn, yxbxwy@gmail.com

***Abstract*—Unmanned Aerial Vehicles (UAVs) are considered as a promising platform providing high-speed wireless communications services. In this paper, we propose a new three-dimensional (3D) non-stationary geometry-based stochastic channel model (GSCM) for the multi-input multi-output (MIMO) communication links between the UAV and the mobile terminal (MT). The proposed GSCM considers not only the 3D scattering scenario, but also the 3D arbitrary trajectories and 3D antenna arrays of both terminals. The computation methods of time evolving channel parameters, i.e., path number, delays, powers and angle parameters, are also given. In addition, the theoretical statistical properties of the proposed GSCM, i.e., the autocorrelation function (ACF), the cross-correlation function (CCF) and the Doppler power spectrum density (DPSD) are analyzed and derived. The good agreement between the simulated results and corresponding theoretical ones shows the correctness of both the simulation and the derivation.**

***Index Terms*—Unmanned Aerial Vehicles (UAVs), non-stationary channel models, geometry-based stochastic channel models (GSCMs), three-dimensional (3D) arbitrary trajectories.**

I. Introduction

During the past decade, there has been a dramatic increase in the use of unmanned aerial vehicles (UAVs), i.e., the remote surveillance, filming, disaster relief, goods transport, and communication relaying, due to their affordable prices, multiple flight controls, high maneuverability, ease operability and increasing payload weight [1]. UAVs also have been considered as the aerial base station in the fifth generation (5G) communication systems [2], [3]. Since multi-input multi-output (MIMO) technologies can improve the capacity and efficiency of communication systems significantly, the UAV communication systems with MIMO technologies have gradually become a research hotspot. However, it is vital to establish accurate and reliable UAV-MIMO channel models for the system design, optimization, and performance evaluation.

This work was supported in part by the National Key Scientific Instrument and Equipment Development Project under Grant No. 2013YQ200607, in part by Natural Science Foundation of China under Grant No. 61631020, in part by the Fundamental Research Funds for the Central Universities under Grant No. NJ20160027, and in part by Open Foundation for Graduate Innovation of NUAA under Grant No. kfjj20170405.

Several channel models for UAV communications can be addressed in [4]–[12]. Among them, the Geometry-based stochastic channel models (GSCMs) [6]–[12] have attracted more and more attention for their good tradeoff between the complexity and accuracy. In [6], [7], the authors proposed two 3D stationary GSCMs for the air-to-ground channels, in which they assumed that scatterers around the mobile terminal (MT) were distributed on the surface of several ellipsoids [6] or cylinders [7] , respectively. In [8], the author took the joint distribution of the azimuth and elevation angles into account and presented a 3D stationary sphere-shaped GSCM. It should be mentioned that the GSCMs in [6]–[8] assumed that all scatterers were fixed for the sake of simplicity. Measurement campaigns [13] have proved that scatterers could appear (birth) or disappear (death) due to the rapid movements of terminals, which has been included in the traditional radio channel models [14]–[17]. Recently, some non-stationary UAV channel models have been presented in [9]–[12]. These models took the time-variant scatterers into account by a birth-death process, but still assumed the UAV is fixed [9], [10] or moving with a constant velocity horizontally [11], [12]. In addition, both terminals are configured with 2D antenna arrays [9]–[11] or uniform linear arrays [12]. However, measurement results in [18] have shown that the flight height of the UAV has a significant effect on the channel characteristic and should not be neglected. This paper aims to fill this gap.

In this paper, we develop a new non-stationary 3D GSCM for UAV-MIMO channels, which allows for 3D arbitrary trajectories and 3D antenna arrays of both terminals. Meanwhile, the corresponding time evolving algorithms of channel parameters, i.e., the path number, delay, power and angle parameters, are also given. In addition, The time-variant autocorrelation function (ACF), cross-correlation function (CCF) and Doppler power spectrum density (DPSD) of the proposed GSCM are investigated and verified by simulations.

The remainder of this paper is organized as follows. In Section II, a new 3D non-stationary GSCM for UAV-MIMO channels as well as the compuatation methods of channel

parameters are presented. The statistical properties of the proposed GSCM are derived in Section III. In Section IV, simulation results are given and compared with the theoretical ones. Finally, conclusions are given in Section V.

II. 3D Non-stationary GSCM for UAV-MIMO Channels

A. Channel impulse response (CIR)

Let us consider the downlink UAV-MIMO channel with Q transmit and P receive antennas as illustrated in Fig. 1. Both terminals are configured with 3D antenna arrays and moving with 3D arbitrary trajectories. In Fig. 1, there are two coordinate systems, i.e., the UAV coordinate system and the MT coordinate system. The coordinate systems are established with the origin at the center of the UAV and MT. The local cluster, denoted by S_n, are composed of M non-uniformly distributed scatterers on the surface of half-sphere with radius R_n centered at the MT, while scatterers around the UAV are neglected. The rest parameters used are listed in Table I.

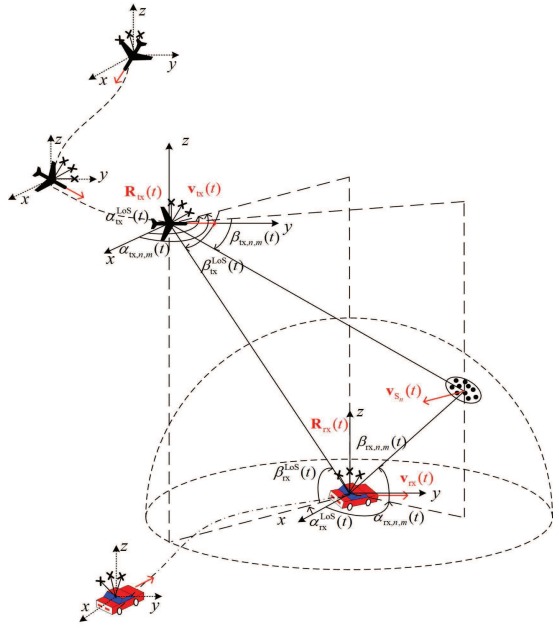

Fig. 1. 3D non-stationary GSCM for UAV-ground link.

The fading channel between the UAV and MT can be expressed as an $Q \times P$ complex matrix, and each element

TABLE I
Parameter definitions in the proposed model

Parameters	Definition
M	Number of scatterers within each cluster
$N(t)$	Number of NLoS paths
$\mathbf{v}_{\mathrm{tx}}(t), \mathbf{v}_{\mathrm{rx}}(t)$	3D velocity vectors of the UAV and MT
$\mathbf{v}_{S_n}(t)$	3D velocity vectors of the cluster S_n
$\phi_{\mathrm{tx/rx}}(t), \theta_{\mathrm{tx/rx}}(t)$	Azimuth and elevation angles of the velocity vector of the UAV or MT
$\alpha^{\mathrm{LoS}}_{\mathrm{tx/rx}}(t), \beta^{\mathrm{LoS}}_{\mathrm{tx/rx}}(t)$	Azimuth and elevation angles of departure/arrival signal of the LoS path
$\alpha_{\mathrm{tx/rx},n}(t), \beta_{\mathrm{tx/rx},n}(t)$	Mean azimuth and elevation angles of departure/arrival of the nth NLoS path
$\alpha_{\mathrm{tx/rx},n,m}(t), \beta_{\mathrm{tx/rx},n,m}(t)$	Azimuth and elevation angles of departure/arrival of the mth ray within the nth NLoS path
$\mathbf{r}_{\mathrm{tx},q}(t), \mathbf{r}_{\mathrm{rx},p}(t)$	3D locations of the qth transmit and pth receive antenna elements
$\mathbf{s}^{\mathrm{LoS}}_{\mathrm{tx}}(t), \mathbf{s}^{\mathrm{LoS}}_{\mathrm{rx}}(t)$	Spherical unit vectors of the LoS path of departure and arrival signals
$\mathbf{s}_{\mathrm{tx},n,m}(t), \mathbf{s}_{\mathrm{rx},n,m}(t)$	Spherical unit vectors of the mth ray within the nth NLoS path of departure and arrival signals

$h_{qp}(t,\tau)$ denotes the complex CIR between the qth transmit antenna and the pth receive antenna. In this paper, we model $h_{qp}(t,\tau)$ as

$$h_{qp}(t,\tau) = \sqrt{P^{\mathrm{LoS}}_{qp}(t)}h^{\mathrm{LoS}}_{qp}(t)\delta(\tau-\tau^{\mathrm{LoS}}_{qp}(t)) + \sum_{n=1}^{N(t)}\sqrt{P^{\mathrm{NLoS}}_{qp,n}(t)}h^{\mathrm{NLoS}}_{qp,n}(t)\delta(\tau-\tau^{\mathrm{NLoS}}_{qp,n}(t)) \tag{1}$$

where $h^{\mathrm{LoS}}_{qp}(t)P^{\mathrm{LoS}}_{qp}(t)$ and $\tau^{\mathrm{LoS}}_{qp}(t)$ mean the complex channel coefficient, the power, and delay of the LoS path, respectively, $h^{\mathrm{NLoS}}_{qp,n}(t)$, $P^{\mathrm{NLoS}}_{qp,n}(t)$ and $\tau^{\mathrm{NLoS}}_{qp,n}(t)$ mean the complex channel coefficient, the power, and delay of the nth NLoS path, respectively. For the LoS path, the complex channel coefficient can be further expressed as

$$h^{\mathrm{LoS}}_{qp}(t) = e^{\mathrm{j}k\left((\mathbf{s}^{\mathrm{LoS}}_{\mathrm{tx}}(t))^T\cdot\mathbf{r}_{\mathrm{tx},q}(t)+(\mathbf{s}^{\mathrm{LoS}}_{\mathrm{rx}}(t))^T\cdot\mathbf{r}_{\mathrm{rx},p}(t)\right)} \cdot e^{\mathrm{j}k\int_0^t\left(\mathbf{v}_{\mathrm{tx}}(t)\cdot\mathbf{s}^{\mathrm{LoS}}_{\mathrm{tx}}(t')+\mathbf{v}_{\mathrm{rx}}(t)\cdot\mathbf{s}^{\mathrm{LoS}}_{\mathrm{rx}}(t')\right)\mathrm{d}t'}e^{\mathrm{j}\phi^{\mathrm{LoS}}} \tag{2}$$

where $k = 2\pi f_0/\mathrm{c}_0$ denotes the wave number, f_0 and c_0 represent the carrier frequency and the speed of light, and ϕ^{LoS} is the random initial phase. For the NLoS path, the complex channel coefficient can be further expressed as (3), where $\phi_{n,m}$ is the random initial phase. In (2) and (3), 3D locations of transmit and receive antenna element can be written as

$$h^{\mathrm{NLoS}}_{qp,n}(t) = \sqrt{\frac{1}{M}}\sum_{m=1}^{M} e^{\left\{\begin{array}{l}\mathrm{j}k\int_0^t\left[(\mathbf{v}_{\mathrm{tx}}(t)-\mathbf{v}_{S_n})\cdot\mathbf{s}_{\mathrm{tx},n,m}(t')+(\mathbf{v}_{\mathrm{rx}}(t)-\mathbf{v}_{S_n})\cdot\mathbf{s}_{\mathrm{rx},n,m}(t')\right]\mathrm{d}t' \\ +\mathrm{j}k\left((\mathbf{s}_{\mathrm{tx},n,m}(t))^T\cdot\mathbf{r}_{\mathrm{tx},q}(t)+(\mathbf{s}_{\mathrm{rx},n,m}(t))^T\cdot\mathbf{r}_{\mathrm{rx},p}(t)\right)+\mathrm{j}\phi_{n,m}\end{array}\right\}} \tag{3}$$

$$\mathbf{R}_{\mathrm{tx/rx}}(t) = \begin{bmatrix} \cos\theta_{\mathrm{tx/rx}}(t)cos\phi_{\mathrm{tx/rx}}(t) & -\sin\phi_{\mathrm{tx/rx}}(t) & -\sin\theta_{\mathrm{tx/rx}}(t)cos\phi_{\mathrm{tx/rx}}(t) \\ \cos\theta_{\mathrm{tx/rx}}(t)\sin\phi_{\mathrm{tx/rx}}(t) & \cos\phi_{\mathrm{tx/rx}}(t) & -\sin\theta_{\mathrm{tx/rx}}(t)\sin\phi_{\mathrm{tx/rx}}(t) \\ \sin\theta_{\mathrm{tx/rx}}(t) & 0 & \cos\theta_{\mathrm{tx/rx}}(t) \end{bmatrix} \tag{4}$$

$\mathbf{r}_{\mathrm{tx},q}(t) = \mathbf{R}_{\mathrm{tx}}(t) \cdot \mathbf{r}_{\mathrm{tx},q}(t_0)$ and $\mathbf{r}_{\mathrm{rx},p}(t) = \mathbf{R}_{\mathrm{rx}}(t) \cdot \mathbf{r}_{\mathrm{rx},p}(t_0)$, here the time-variant rotation matrix $\mathbf{R}_{\mathrm{tx}}(t)$ and $\mathbf{R}_{\mathrm{rx}}(t)$ are introduced to take the effect of 3D arbitrary trajectories into account and defined as (4).

B. Flowchart of updating channel parameters

Fig. 2 gives the updating process of channel parameters for the proposed model and it can be described as follows:

Step 1: Generate the total number of NLoS paths based on the birth-death process at time instant t.

Step 2: Generate initial clusters and scatterers randomly at time instant t. The computation method of channel parameters, i.e., delays, powers and angle parameters, is given in Section III-B.

Step 3: For the newly generated path, the geometrical parameter is generated similar to the initial cluster. For the survival path, the geometrical parameter is updated by the method in Section III-B.

Step 4: When the evolution at time t is finished, the algorithm returns to Step 1 for the next time instant.

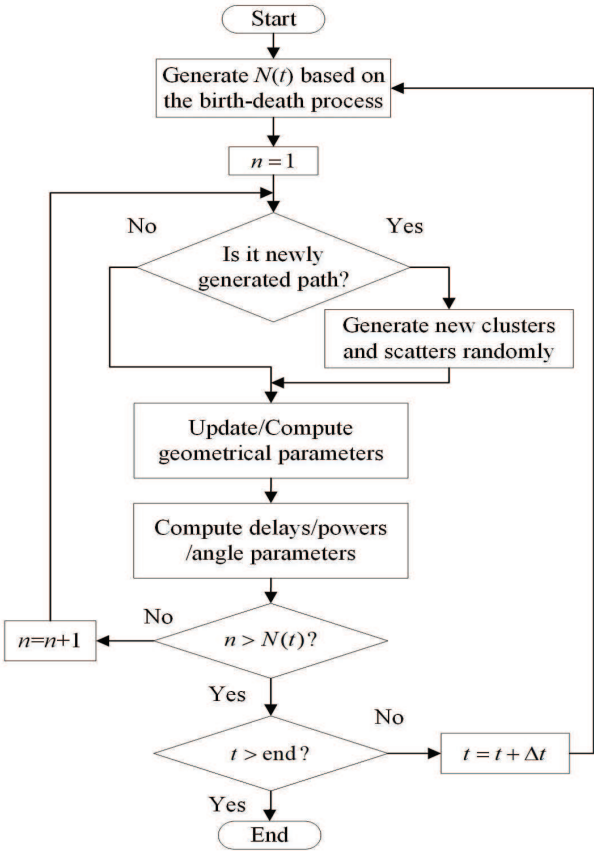

Fig. 2. Flowchart of updating channel parameters.

C. Computation methods of channel parameters

1) Total number of NLoS paths: In this paper, we model the birth-death process of NLoS paths by a Markov process, where the birth and death rates of clusters are λ_{B} and λ_{D}, respectively. We assume that the UAV, MT, and each cluster move at constant speeds in the time interval Δt and mean velocities of clusters are denoted as $\mathbf{v}_{\mathrm{S}}(t) = \mathrm{E}\{\mathbf{v}_{\mathrm{S}_n}(t)\}$. The channel fluctuation $\varepsilon(t, \Delta t)$ measures how much the scattering environment varies within a short period. Since the variation of scattering environment is due to the movements of the UAV, MT and clusters during the time span from t to $t + \Delta t$, the time dependent channel fluctuation can be calculated as

$$\varepsilon(t, \Delta t) = \left(\|\mathbf{v}_{\mathrm{tx}}(t)\| + \|\mathbf{v}_{\mathrm{rx}}(t)\| + P_{\mathrm{c}} \|\mathbf{v}_{\mathrm{S}}(t)\|\right) \Delta t \quad (5)$$

where P_{c} denotes the average probability of moving clusters.

The survival probability of NLoS paths is computed as

$$P_{\mathrm{r}}(t, \Delta t) = e^{-\lambda_{\mathrm{B}} \frac{\varepsilon(t, \Delta t)}{D_{\mathrm{c}}}} \quad (6)$$

where D_c denotes a scenario dependent coefficient describing the space correlation. The expectation of the total number of NLoS paths can be calculated by

$$E\{N(t)\} = \frac{\lambda_{\mathrm{D}}}{\lambda_{\mathrm{B}}} \quad (7)$$

where $\mathrm{E}\{\cdot\}$ denotes the statistical average.

2) Geometrical parameters: For newly generated clusters, the 3D location vectors and velocities of clusters can be obtained by measurement campaigns or generation randomly. For the survived clusters, the 3D location vectors of the UAV, MT and cluster S_n at the time instant t can be updated by

$$\mathbf{L}_{\mathrm{tx/rx/S}_n}(t) = \mathbf{L}_{\mathrm{tx/rx/S}_n}(t - \Delta t) + \mathbf{v}_{\mathrm{tx/rx/S}_n}(t)\Delta t \quad (8)$$

where $\mathbf{L}_{\mathrm{tx}}(t)$, $\mathbf{L}_{\mathrm{rx}}(t)$ and $\mathbf{L}_{S_n}(t)$ denote the time-variant 3D location vectors of the UAV, MT and cluster S_n, respectively. The initial location vectors can be calculated by $\mathbf{L}_{\mathrm{tx}}(t_0) = D^{\mathrm{LoS}}(t_0)\mathbf{s}_{\mathrm{tx}}^{\mathrm{LoS}}(t_0)$, $\mathbf{L}_{\mathrm{rx}}(t_0) = D^{\mathrm{LoS}}(t_0)\mathbf{s}_{\mathrm{rx}}^{\mathrm{LoS}}(t_0)$ and $\mathbf{L}_{S_n}(t_0) = R_n \mathbf{s}_{\mathrm{rx},n}(t_0)$, where $D^{\mathrm{LoS}}(t_0)$ means the initial value of the distance of the LoS path.

By using the transform from the Cartesian coordination to spherical coordination, the mean elevation angle of departure (EAoD) and arrival (EAoA), azimuth angle of departure (AAoD) and arrival (AAoA) of the LoS path can be calculated by

$$\beta_{\mathrm{tx/rx}}^{\mathrm{LoS}}(t) = \arctan\left(\frac{\mathbf{L}^z_{\mathrm{rx/tx}}(t) - \mathbf{L}^z_{\mathrm{tx/rx}}(t)}{\sqrt{\left(\mathbf{L}^x_{\mathrm{tx/rx}}(t) - \mathbf{L}^x_{\mathrm{rx/tx}}(t)\right)^2 + \left(\mathbf{L}^y_{\mathrm{tx/rx}}(t) - \mathbf{L}^y_{\mathrm{rx/tx}}(t)\right)^2}}\right) \quad (9)$$

and

$$\alpha_{\mathrm{tx/rx}}^{\mathrm{LoS}}(t) = \arctan\left(\frac{\mathbf{L}^y_{\mathrm{rx/tx}}(t) - \mathbf{L}^y_{\mathrm{tx/rx}}(t)}{\sqrt{\left(\mathbf{L}^x_{\mathrm{tx/rx}}(t) - \mathbf{L}^x_{\mathrm{rx/tx}}(t)\right)^2 + \left(\mathbf{L}^y_{\mathrm{tx/rx}}(t) - \mathbf{L}^y_{\mathrm{rx/tx}}(t)\right)^2}}\right) \quad (10)$$

where $\mathbf{L}^x_{\mathrm{tx/rx/S}_n}(t)$, $\mathbf{L}^y_{\mathrm{tx/rx/S}_n}(t)$ and $\mathbf{L}^z_{\mathrm{tx/rx/S}_n}(t)$ are the x, y and z components of $\mathbf{L}_{\mathrm{tx/rx/S}_n}(t)$, respectively.

Similarly, the mean EAoD, EAoA and AAoD, AAoA of nth NLoS path at time instant t can be calculated by

$$\beta_{\mathrm{rx/tx},n}(t) = \arctan\left(\frac{\mathbf{L}^z_{\mathrm{S}_n}(t) - \mathbf{L}^z_{\mathrm{rx/tx}}(t)}{\sqrt{\left(\mathbf{L}^x_{\mathrm{S}_n}(t) - \mathbf{L}^x_{\mathrm{rx/tx}}(t)\right)^2 + \left(\mathbf{L}^y_{\mathrm{S}_n}(t) - \mathbf{L}^y_{\mathrm{rx/tx}}(t)\right)^2}}\right) \quad (11)$$

and

$$\alpha_{\mathrm{rx/tx},n}(t) = \arctan\left(\frac{\mathbf{L}^{y}_{\mathrm{S}_n}(t)-\mathbf{L}^{y}_{\mathrm{rx/tx}}(t)}{\sqrt{(\mathbf{L}^{x}_{\mathrm{S}_n}(t)-\mathbf{L}^{x}_{\mathrm{rx/tx}}(t))^2+(\mathbf{L}^{y}_{\mathrm{S}_n}(t)-\mathbf{L}^{y}_{\mathrm{rx/tx}}(t))^2}}\right). \quad (12)$$

3) Path delays and powers: The time-variant delay of the LoS path can be calculated as

$$\tau^{\mathrm{LoS}}_{qp}(t) = \left\|\mathbf{L}_{\mathrm{tx}}(t) - \mathbf{L}_{\mathrm{rx}}(t)\right\|/\mathrm{c} \quad (13)$$

and the time-variant delay of *n*th NLoS path can be calculated as

$$\tau^{\mathrm{NLoS}}_{qp,n}(t) = \underbrace{\left\|\mathbf{L}_{\mathrm{tx}}(t) - \mathbf{L}_{\mathrm{S}_n}(t)\right\|/c}_{\tau^{\mathrm{NLoS}}_{tx,qp,n}(t)} + \underbrace{\left\|\mathbf{L}_{\mathrm{S}_n}(t) - \mathbf{L}_{\mathrm{rx}}(t)\right\|/c}_{\tau^{\mathrm{NLoS}}_{rx,qp,n}(t)}. \quad (14)$$

Then, the time-variant power of the LoS path can be calculated as [19]

$$P^{\mathrm{LoS}}_{qp}(t) = exp\left(-\tau^{\mathrm{LoS}}_{qp}(t)\frac{1-r_\tau}{r_\tau\sigma_\tau}\right)10^{\frac{Y_n}{10}} \quad (15)$$

where r_τ and σ_τ mean the delay scalar and delay spread, and Y_n follows the Gaussian distribution characterizing the magnitude large-scale fading in dB. Meanwhile, the power of the *n*th NLoS path can be calculated by

$$P^{\mathrm{NLoS}}_{qp,n}(t) = exp\left(-\tau^{\mathrm{NLoS}}_{qp,n}(t)\frac{1-r_\tau}{r_\tau\sigma_\tau}\right)10^{\frac{Y_n}{10}}. \quad (16)$$

Therefore, the ratio of the power of LoS path to the total power of all NLoS paths, namely the Ricean factor, can be calculated as

$$K(t) = \frac{P^{\mathrm{LoS}}_{qp}(t)}{\sum_{n=1}^{N(t)} P^{\mathrm{NLoS}}_{qp,n}(t)}. \quad (17)$$

4) Angle parameters: In this paper, we jointly consider the azimuth and elevation angles and model them by the von Mises Fisher (VMF) distribution [12],

$$p(\alpha,\beta) = \frac{\mathrm{e}^{\kappa\left(cos\beta\cos\bar{\beta}\cos(\alpha-\bar{\alpha})+sin\beta sin\bar{\beta}\right)}}{(\kappa^{-1/2})(2\pi)^{3/2}\mathrm{I}_{1/2}(\kappa)} \quad (18)$$

where $\bar{\alpha}$ and $\bar{\beta}$ are the mean azimuth and elevation angles, $\mathrm{I}_{1/2}(\cdot)$ denotes the zero-order modified Bessel function, and κ controls the concentration of the distribution. In a scattering environment, as $\kappa \to \infty$ the scattering becomes a point source and when $\kappa = 0$ the isotropic scattering occurs.

Then, angle parameters EAoA and AAoA of the mth ray within nth path can be calculated by adding the angle offset $\Delta\alpha$ and $\Delta\beta$ as

$$[\beta_{\mathrm{rx},n,m}(t), \alpha_{\mathrm{rx},n,m}(t)] = [\beta_{\mathrm{rx},n}(t), \alpha_{\mathrm{rx},n}(t)] + [\Delta\beta, \Delta\alpha] \quad (19)$$

where $\Delta\alpha$ and $\Delta\beta$ also obey the VMF distribution. Angle parameters EAoD and AAoD of the mth ray of nth path can be calculated by

$$\alpha_{\mathrm{tx},n,m}(t) = \arctan\left(\frac{\mathbf{L}^{y}_{\mathrm{S}_{n,m}}(t)-\mathbf{L}^{y}_{\mathrm{tx}}(t)}{\sqrt{(\mathbf{L}^{x}_{\mathrm{S}_{n,m}}(t)-\mathbf{L}^{x}_{\mathrm{tx}}(t))^2+(\mathbf{L}^{y}_{\mathrm{S}_{n,m}}(t)-\mathbf{L}^{y}_{\mathrm{tx}}(t))^2}}\right) \quad (20)$$

and

$$\beta_{\mathrm{tx},n,m}(t) = \arctan\left(\frac{\mathbf{L}^{z}_{\mathrm{S}_{n,m}}(t)-\mathbf{L}^{z}_{\mathrm{tx}}(t)}{\sqrt{(\mathbf{L}^{x}_{\mathrm{S}_{n,m}}(t)-\mathbf{L}^{x}_{\mathrm{tx}}(t))^2+(\mathbf{L}^{y}_{\mathrm{S}_{n,m}}(t)-\mathbf{L}^{y}_{\mathrm{tx}}(t))^2}}\right) \quad (21)$$

where the location vector of each scatter within *n*th cluster can be expressed as $\mathbf{L}_{\mathrm{S}_{n,m}}(t) = R_n\mathbf{s}_{\mathrm{rx},n,m}(t)$.

III. Statistical Properties of the Proposed GSCM

1) ACF: The time-variant transfer function of the channel is defined as the Fourier transform of the time-variant CIR $h_{qp}(t,\tau)$ with respect to the propagation delay can be defined as

$$H_{qp}(\mathbf{r}, f, t) = \int_{-\infty}^{\infty} h_{qp}(t,\tau)\mathrm{e}^{-\mathrm{j}2\pi f\tau}\mathrm{d}\tau \quad (22)$$

where $\mathbf{r} = \{\Delta\mathbf{r}_{\mathrm{tx}}, \Delta\mathbf{r}_{\mathrm{rx}}\}$ is the space lag, and $\Delta\mathbf{r}_{\mathrm{tx}} = \mathbf{r}_{\mathrm{tx},q_2} - \mathbf{r}_{\mathrm{tx},q_1}$ and $\Delta\mathbf{r}_{\mathrm{rx}} = \mathbf{r}_{\mathrm{rx},p_2} - \mathbf{r}_{\mathrm{rx},p_1}$ denote the spacing between antenna elements at the UAV and MT. In this paper, we assume the UAV channel is non-stationary only on time domain. Thus, the normalized 3D spatial-temporal correlation function can be simplified as

$$\rho_{q_1p_1,q_2p_2}(\Delta t; t) = E\left\{\frac{H^*_{q_1p_1}(t)H_{q_2p_2}(t+\Delta t)}{\left|H^*_{q_1p_1}(t)\right|\left|H_{q_2p_2}(t+\Delta t)\right|}\right\} \quad (23)$$

where $(\cdot)^*$ denotes the complex conjugation operation. Moreover, the LoS and NLoS paths are usually uncorrelated, and thus (23) can be rewritten as

$$\rho_{q_1p_1,q_2p_2}(\Delta t; t) = \rho^{\mathrm{LoS}}_{q_1p_1,q_2p_2}(\Delta t; t) + \rho^{\mathrm{NLoS}}_{q_1p_1,q_2p_2,n}(\Delta t; t). \quad (24)$$

The effect of survival probability from t to $t+\Delta t$ should be taken into account and the ACF can be obtained by substituting (22) into (23) and imposing $q_1 = q_2 = q$ and $p_1 = p_2 = p$

$$\rho_{qp}(\Delta t; t) = \rho^{\mathrm{LoS}}_{qp}(\Delta t; t) + \rho^{\mathrm{NLoS}}_{qp,n}(\Delta t; t) \quad (25)$$

where

$$\rho^{\mathrm{LoS}}_{qp}(\Delta t; t) = \frac{K(t)}{K(t)+1}h^{\mathrm{LoS}*}_{qp}(t)\mathrm{e}^{\mathrm{j}2\pi f\tau^{\mathrm{LoS}}_{qp}(t)} \cdot h^{\mathrm{LoS}}_{qp}(t+\Delta t)\mathrm{e}^{-\mathrm{j}2\pi f\tau^{\mathrm{LoS}}_{qp}(t+\Delta t)} \quad (26)$$

and

$$\rho_{qp,n}^{\mathrm{NLoS}}(\Delta t;t)=\frac{P_{\mathrm{r}}}{K(t)+1}\mathrm{E}\left[\begin{array}{l}h_{qp,n}^{\mathrm{NLoS}*}(t)h_{qp,n}^{\mathrm{NLoS}}(t+\Delta t)\\ \cdot\mathrm{e}^{\mathrm{j}2\pi f\tau_{qp,n}(t)}\mathrm{e}^{-\mathrm{j}2\pi f\tau_{qp,n}(t+\Delta t)}\end{array}\right]. \tag{27}$$

2) CCF: By imposing $\Delta t=0$ in (23), we can obtain the CCF between two channel coefficients as

$$\rho_{q_1p_1,q_2p_2}(\{\Delta\mathbf{r}_{\mathrm{tx}},\Delta\mathbf{r}_{\mathrm{rx}}\};t)=\rho_{q_1p_1,q_2p_2}^{\mathrm{LoS}}(\{\Delta\mathbf{r}_{\mathrm{tx}},\Delta\mathbf{r}_{\mathrm{rx}}\};t)+\rho_{q_1p_1,q_2p_2,n}^{\mathrm{NLoS}}(\{\Delta\mathbf{r}_{\mathrm{tx}},\Delta\mathbf{r}_{\mathrm{rx}}\};t) \tag{28}$$

where

$$\rho_{q_1p_1,q_2p_2}^{\mathrm{LoS}}(\{\Delta\mathbf{r}_{\mathrm{tx}},\Delta\mathbf{r}_{\mathrm{rx}}\};t)=\frac{K(t)}{K(t)+1}h_{q_1p_1}^{\mathrm{LoS}*}(t)h_{q_2p_2}^{\mathrm{LoS}}(t)\cdot\mathrm{e}^{\mathrm{j}2\pi f\tau_{q_1p_1}^{\mathrm{LoS}}(t)}\mathrm{e}^{-\mathrm{j}2\pi f\tau_{q_2p_2}^{\mathrm{LoS}}(t)} \tag{29}$$

and

$$\rho_{q_1p_1,q_2p_2,n}^{\mathrm{NLoS}}(\{\Delta\mathbf{r}_{\mathrm{tx}},\Delta\mathbf{r}_{\mathrm{rx}}\};t)=\frac{P_{\mathrm{r}}}{K(t)+1}\cdot\mathrm{E}[h_{q_1p_1,n}^{\mathrm{NLoS}*}(t)\mathrm{e}^{\mathrm{j}2\pi f\tau_{q_1p_1,n}(t)}h_{q_2p_2,n}^{\mathrm{NLoS}}(t)\mathrm{e}^{-\mathrm{j}2\pi f\tau_{q_2p_2,n}(t)}]. \tag{30}$$

3) DPSD: The DPSD of conventional stationary channels is defined by the Fourier transform of the ACF, but this method is invalid for non-stationary processes. We redefine the DPSD as the short-time DPSD which can be calculated by the squared amplitude of signals short-time Fourier transform (STFT) as

$$S_{qp}(f;t)=\left|\int_{-\infty}^{\infty}\rho_{qp}(\Delta t;t)e^{-\mathrm{j}2\pi f\Delta t}\nu(t-\Delta t)\mathrm{d}\Delta t\right|^2 \tag{31}$$

where $\nu(t-\Delta t)$ is the window function, which is sufficiently short such that the process can be considered to be stationary.

IV. Simulation Results and Validation

In this section, we validate the theoretical statistical properties of the proposed GSCM by simulation method under the C2-LoS scenario [19]. The time variant velocity and direction are modeled as $\left\|\mathbf{v}_{\mathrm{tx/rx}}(t)\right\|=v_{\mathrm{tx/rx}}+a_{\mathrm{tx/rx}}\cdot t$, $\phi_{\mathrm{tx/rx}}(t)=\varphi_{\mathrm{tx/rx}}+\alpha_{\mathrm{tx/rx}}\cdot t$ and $\theta_{\mathrm{tx/rx}}(t)=\vartheta_{\mathrm{tx/rx}}+\beta_{\mathrm{tx/rx}}\cdot t$, where $v_{\mathrm{tx/rx}}$ and $a_{\mathrm{tx/rx}}$ are the initial velocity and acceleration of the UAV and MT, $\varphi_{\mathrm{tx/rx}}$ and $\vartheta_{\mathrm{tx/rx}}$ are the initial azimuth and elevation angle of motion of the UAV and MT, respectively, $\alpha_{\mathrm{tx/rx}}$ and $\beta_{\mathrm{tx/rx}}$ are the corresponding angular speed. The detailed simulation parameters are given in Table II.

By using (23)-(27), the absolute values of the theoretical ACFs at three time instants t= 0s, 2s, and 4s are calculated and given in Fig. 3(a). For comparison purpose, the corresponding simulated ACFs are also shown in Fig. 3(a). Similarly, by using (28)-(30), the theoretical CCFs and corresponding simulated CCFs at three time instants t= 0s, 2s, and 4s are shown in Fig. 3(b). In this figure, the y axis has been normalized with respect to half wavelength. It can be observed that the

TABLE II
Simulation Parameters

Parameters	Values	Parameters	Values
λ_{D}	28/m	λ_{B}	14/m
P_c	0.3	Δt	1ms
R	$U(60,80)m$	κ	0.5
f_c	2.4GHz	$D^{\mathrm{LoS}}(t_0)$	200m
D_c	80m	$\|\mathbf{v}_S\|$	1.4m/s
v_{tx}	27m/s	a_{tx}	$0.02\mathrm{m/s}^2$
v_{rx}	8m/s	a_{rx}	$0.001\mathrm{m/s}^2$
φ_{tx}	130°	α_{tx}	30°/s
φ_{rx}	10°	α_{rx}	2°/s
ϑ_{tx}	20°	β_{tx}	3°/s
ϑ_{rx}	5°	β_{rx}	0.2°/s
$\alpha_{\mathrm{rx}}^{\mathrm{LoS}}(t_0)$	10°	$\beta_{\mathrm{rx}}^{\mathrm{LoS}}(t_0)$	80°
$\beta_{\mathrm{rx},n}(t_0)$	random	$\alpha_{\mathrm{rx},n}(t_0)$	random
r_τ	2.5	σ_τ	41ns

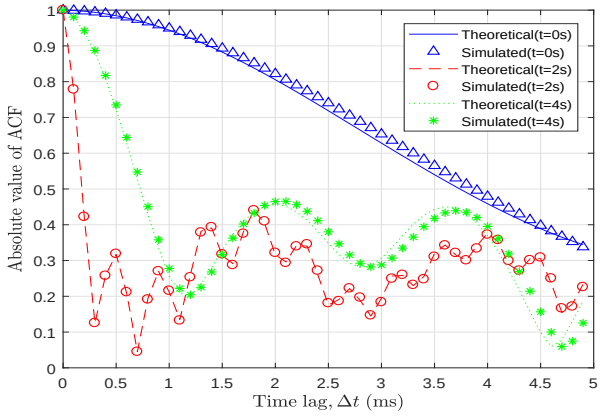

(a)

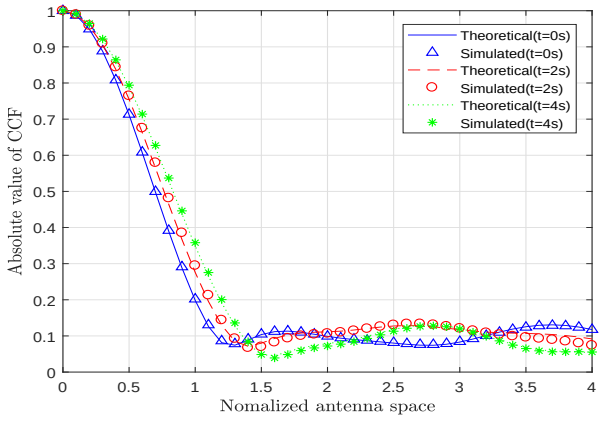

(b)

Fig. 3. (a) Theoretical and simulated ACFs at different time instants. (b) Theoretical and simulated CCFs at different time instants.

ACF and CCF change over time due to time-variant channel parameters, and the good consistent between theoretical results and simulation results in both Fig. 3(a) and Fig. 3(b) verify the correctness of above derivations.

By using (31), the theoretical DPSDs are calculated and given by Fig. 4(a). For comparison purpose, the theoretical

DPSDs at three time instants are extracted from Fig. 4(a) and the corresponding simulated DPSDs are shown in Fig. 4(b). The drift of DPSDs over time due to the movements of the UAV, MT and clusters can be clearly observed. It also can be seen that Fig. 4 has an asymmetric DPSD, which is the consequence of the non-isotropic scattering environment. Again, the simulation results align well with the theoretical results, illustrating the correctness of the derivations.

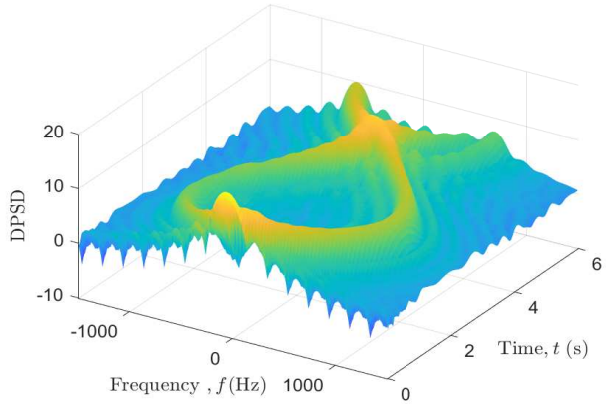

(a)

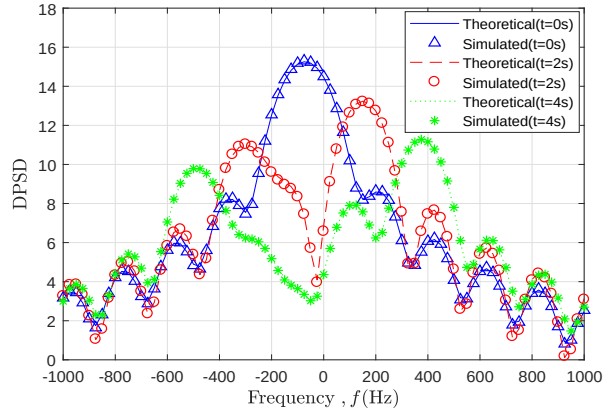

(b)

Fig. 4. (a) Theoretical time-variant DPSDs. (b) Theoretical and simulated DPSDs at different time instants.

V. Conclusions

In this paper, we have proposed a 3D half-sphere GSCM for UAV-MIMO channels incorporating 3D arbitrary trajectories and 3D antenna arrays of both terminals. The update and computation methods of time-variant channel parameters have been developed and analyzed. Based on the proposed model, the expressions of time-variant statistical properties such as the ACF, CCF and DPSD have also been derived. The good agreement between the theoretical derived ones and simulation results has validated the utility of the proposed model. Therefore, the proposed model are very helpful on the performance evaluation and system optimization of the UAV-based wireless communication systems.

References

[1] Y. Zeng, R. Zhang, J. L. Teng, "Wireless communications with unmanned aerial vehicles: opportunities and challenges," *IEEE Commun. Mag.*, vol. 54, no. 5, pp. 36–42, May 2016.

[2] Z. Feng, C. Qiu, Z. Feng, "An effective approach to 5G: Wireless network virtualization," *IEEE Commun. Mag.*, vol. 53, no. 12, pp. 53–59, 2015.

[3] C.-X Wang, J. BIAN, J. SUN, W. ZHANG and M. ZHANG, "A survey of 5G channel measurements and models," *IEEE Commun. Surv. & Tutor.*, in press.

[4] Z. Shi, P. Xia, Z. Gao, L. Huang, and C. Chen, "Modeling of wireless channel between UAV and vessel using the fdtd method," in *Proc. WiCOM*, Beijing, China, Sept. 2014, pp. 100–104.

[5] M. Simunek, F. P. Fontan, P. Pechac, "The UAV low elevation propagation channel in urban areas: Statistical analysis and time-series generator," *IEEE Trans. Antennas Propag.*, vol. 61, no. 7, pp. 3850–3858, Apr. 2013.

[6] S. M. Gulfam, S. J. Nawaz, A. Ahmed, "A novel 3D analytical scattering model for air-to-ground fading channels," *Appl. Sci.*, vol. 6, no. 8, pp. 207–228, Aug. 2016.

[7] Y. Li, X. Cheng, "New deterministic and statistical simulation models for non-isotropic UAV-MIMO channels," in *Proc. Wirel. Commun. and Signal Process.*, Nanjing, China, Oct. 2017, pp. 1–6.

[8] K. Jin, X. Cheng, X. Ge, "Three dimensional modeling and space-time correlation for UAV channels," in *Proc. IEEE Veh. Technol. Conf.*, Sydney, Australia, June 2017, pp. 1–5.

[9] Z. Lian, L. Jiang, C. He, "A 3-D wideband model based on dynamic evolution of scatterers for HAP-MIMO channel," *IEEE Commun. Lett.*, vol. 21, no. 3, pp. 684–687, Dec. 2017.

[10] J. Hu, L. Jiang, C. He, "A 3-D HAP-MIMO channel model based on dynamic properties of scatterers," in *Proc. Wirel. Commun. and Signal Process.*, Nanjing, China, Dec. 2017, pp. 1–5.

[11] Z. Lian, L. Jiang, C. He, "A novel channel model for 3-D HAP-MIMO communication systems," in *Proc. NaNA*, Hakodate, Japan, Sep. 2016, pp. 1–6.

[12] Q. Zhu, K. Jiang, X. Chen, W. Zhong, Y. Yang, "A novel 3D non-stationary UAV-MIMO channel model and its statistical properties," *China Commun.*, in Press.

[13] D. W. Matolak, R. Sun, "AirCground channel characterization for unmanned aircraft systemsłPart I: Methods, measurements, and models for over-water settings," *IEEE Trans. Veh. Technol.*, vol. 66, no. 1, pp. 26–44, June 2017.

[14] Q. Zhu, H. Li, Y. Fu, "A novel 3D non-stationary wireless MIMO channel simulator and hardware emulator," *IEEE Trans. Commun.*, pp. 1–14, 2018, DOI 10.1109/TCOMM.2018.2824817.

[15] S. Wu, C.-X Wang, M. Aggoune M, "A general 3D non-stationary 5G wireless channel model," *IEEE Trans. Commun.*, vol. 66, no. 7, pp. 1–14, July 2018.

[16] K. Jiang, X. Chen, Q. Zhu, L. Chen, D. Xu, B. Chen, "A novel simulation model for non-stationary rice fading channels," *Wirel. Commun. Mobile Comput.*, vol. 2018, no. 1, pp. 1–9, 2018.

[17] Q. Zhu, Y. Yang, X. Chen, Y. Tan, Y. Fu, C.-X Wang, W. Li, "A novel 3D non-stationary vehicle-to-vehicle channel model and its spatial-temporal correlation properties," *IEEE Access*, in Press.

[18] R. Sun, D. W. Matolak, "Air-ground channel characterization for unmanned aircraft systems part II: Hilly and mountainous settings," *IEEE Trans. Veh. Technol.*, vol. 66, no. 3, pp. 1913–1925, June 2017.

[19] J. Meinila, P. Kyosti, L. Hentila, "WINNER+ fnal channel models," 2010, http://projects.celtic-initiative.org/winner+/